

Constraint-Aware Discrete-Time PID Gain Optimization for Robotic Joint Control Under Actuator Saturation

Ojasva Mishra¹ Xiaolong Wu² Min Xu^{2*}

¹Downington STEM Academy, Downington, PA, USA

²Carnegie Mellon University, School of Computer Science, Pittsburgh, PA, USA

February 6, 2026

Abstract

The precise regulation of rotary actuation is fundamental in autonomous robotics, yet practical PID loops deviate from continuous-time theory due to discrete-time execution, actuator saturation, and small delays and measurement imperfections. We present an implementation-aware analysis and tuning workflow for saturated discrete-time joint control. We (i) derive PI stability regions under Euler and exact zero-order-hold (ZOH) discretizations using the Jury criterion, (ii) evaluate a discrete back-calculation anti-windup realization under saturation-dominant regimes, and (iii) propose a hybrid-certified Bayesian optimization workflow that screens analytically unstable candidates and behaviorally unsafe transients while optimizing a robust IAE objective with soft penalties on overshoot and saturation duty. Baseline sweeps ($\tau = 1.0$ s, $\Delta t = 0.01$ s, $u \in [-10, 10]$) quantify rise/settle trends for P/PI/PID. Under a randomized model family emulating uncertainty, delay, noise, quantization, and tighter saturation, robustness-oriented tuning improves median IAE from 0.687 to 0.470 while keeping median overshoot below 2%. In simulation-only tuning, the certification screen rejects 11.6% of randomly sampled gains within bounds before full robust evaluation, improving sample efficiency without hardware experiments.

Keywords: PID control, discrete-time implementation, actuator saturation, integral windup, anti-windup, robustness, Jury stability, Bayesian optimization, robotic joints

1 Introduction

The precise regulation of rotary actuation constitutes a fundamental challenge in the engineering of autonomous robotic systems, ranging from industrial manipulators to self-guided electric vehicle charging mechanisms. In these cyber-physical domains, the fidelity of motion control

determines the operational success of the system. The Proportional-Integral-Derivative (PID) controller remains a widely used standard in feedback control systems due to its versatile structure and proven capacity to ensure asymptotic stability.

Despite the ubiquity of PID control, the translation of continuous-time control theory into physical application is frequently complicated by hardware constraints. Theoretical models often assume infinite control authority and continuous signal processing; however, practical robotic joints operate within strict voltage/torque limits and utilize digital processors that execute control laws in discrete time steps. When a controller demands an input that exceeds the physical capabilities of the actuator, the system enters a regime of saturation, introducing non-linearities that can degrade performance or induce instability. In addition, real embedded loops exhibit non-idealities such as computation delay, sensor noise, and encoder quantization that interact with discretization and saturation.

This research presents a systematic characterization of a first-order Linear Time-Invariant (LTI) robotic joint under discrete PID control. Unlike generalized derivations found in introductory literature, this study isolates the specific impact of control gains (K_p , K_i , and K_d) within the context of a magnitude-constrained system and then extends the analysis toward robust, implementation-aware tuning in simulation.

Contributions

While the baseline gain sweeps are intended to be interpretable, the paper is strengthened by three contributions that directly target robotics implementation gaps:

1. Closed-form PI stability regions in discrete time.

For a first-order joint model, we derive explicit gain- and sampling-dependent stability constraints for PI control using the Jury criterion under both forward-Euler and exact ZOH discretizations, enabling “safe” gain selection before simulation.

*Corresponding author.

2. Saturation-dominant evaluation with anti-windup.

We include a discrete back-calculation anti-windup update and demonstrate how it changes recovery dynamics when saturation is frequent (a regime not captured by small-step, low-demand baselines).

3. Robust constraint-aware gain selection.

We propose a robustness-oriented Bayesian gain-selection workflow that optimizes IAE while enforcing stability and soft constraints on overshoot and saturation duty across a randomized family of joint models (delay, noise, quantization, and parameter uncertainty).

2 Motivation

2.1 Problem formulation

While the Proportional-Integral-Derivative (PID) controller is the theoretic standard for asymptotic stability in linear time-invariant (LTI) systems, its implementation in robotic actuation is frequently compromised by physical nonlinearities—specifically actuator saturation and discretization artifacts. Theoretical derivations often assume continuous-time signal processing and infinite control authority. However, practical autonomous joints operate within strict voltage limits (u_{\min}, u_{\max}) and utilize digital processors that execute control laws in discrete time steps (Δt). The discrepancy between continuous-time theory and discrete-time implementation creates a performance gap. When a high-gain controller demands an input exceeding the actuator’s physical capacity ($|u(t)| > u_{\text{sat}}$), the system enters a regime of saturation. This introduces windup phenomena and nonlinear transient behaviors that degrade tracking fidelity, represented by the Integral of Absolute Error (IAE) and settling time. Furthermore, the use of first-order forward Euler discretization in low-latency embedded loops introduces numerical approximations that deviate from ideal analytical predictions [2, 3].

2.2 Research objectives

The primary objective of this study is to systematically characterize the dynamic response of a first-order LTI robotic joint under magnitude-constrained discrete PID control and to extend the analysis toward robust practice without requiring hardware access.

Specifically, this research aims to:

1. Quantify discretization sensitivity: analyze the deviation between theoretical continuous-time predictions and discrete-time implementations using Forward Euler integration with limited sampling resolution ($\Delta t = 0.01$ s).

Table 1: Key symbols used throughout this paper with the equation number of introduction marked.

Symbol	Description
$y(t), y_k$	Joint output (position) in continuous and discrete time; plant output in (1)–(3).
$u(t), u_k$	Control effort; proportional/PI/PID laws in (4)–(6).
r	Reference (desired joint position), unit step used throughout baseline experiments.
e_k	Tracking error, $e_k = r - y_k$, defined after (3).
τ	Plant time constant in the first-order model (1).
K	Plant static gain in (1).
Δt	Sampling interval (control period) in (3).
K_p, K_i, K_d	Proportional, integral, and derivative gains in (4)–(6).
I_k	Discrete integral state and back-calculation update in (8).
u_{\min}, u_{\max}	Actuator saturation bounds used in the clamp (7).
$\%OS$	Percent overshoot metric in (9).
t_r, t_s	Rise time and settling time in (10) and (11).
e_{ss}	Terminal steady-state error estimate in (12).
IAE	Integral of absolute error in (13).
z	Discrete-time closed-loop pole for P control in (14).
a, b	Exact ZOH discrete-time coefficients in (23).
K_{aw}	Anti-windup (back-calculation) gain in (8).
J	Robust BO objective in (21).
$\lambda_{os}, \lambda_{sat}, \lambda_u$	BO penalty weights in (21).

2. Characterize saturation nonlinearities: evaluate the impact of control effort clamping ($u_k \in [-10, 10]$) on integral windup and rise-time performance during step responses, including saturation-dominant tasks.
3. Derive constraint-aware tuning heuristics: establish tuning guidelines for K_p, K_i, K_d that minimize IAE while enforcing stability and bounded overshoot under model variations (delay, noise, parameter uncertainty).

3 Related work

This paper connects three threads that frequently appear in robotics actuation but are often studied in isolation: (i) digital PID implementation effects (sampling and discretization), (ii) saturation and anti-windup behavior in voltage/torque-limited joints, and (iii) data-efficient gain selection under uncertainty when direct hardware iteration is impractical.

3.1 Digital PID in robotics and sampled-data effects

PID remains a workhorse in robotics because it is simple, interpretable, and effective across a wide range of actuators.

ation plants. Recent reviews and sampled-data surveys emphasize that real closed-loop behavior depends strongly on implementation details that are frequently abstracted away in continuous-time analysis, including sampling, numerical discretization, delays, quantization, and actuator limits [1, 2]. In embedded joint control, the sampling period is not a nuisance parameter: it directly shapes phase margin and can turn a seemingly benign continuous-time tuning into an unstable discrete-time loop.

Most classical PID tuning recipes are formulated in continuous time and then discretized heuristically. In contrast, we explicitly characterize discrete-time stability for the PI subset under forward-Euler discretization, yielding gain- and sampling-dependent stability regions (Sec. 4.3). This complements simulation sweeps by providing an analytic constraint that can be checked before running expensive trials and that can be used to prune unsafe regions of the search space.

3.2 Saturation, integral windup, and anti-windup compensation

When a commanded effort exceeds actuator bounds, the loop becomes nonlinear and integral windup can dominate settling behavior, producing long recovery tails and overshoot once the actuator leaves saturation. Contemporary anti-windup work continues to refine compensation mechanisms (including back-calculation and two-stage designs) that explicitly account for saturation, quantization, and embedded implementation constraints [4–6]. In robotics, where large setpoint steps and load disturbances are common, windup is not a rare failure mode but a routine operating condition.

Our contribution is not a new anti-windup law, but a robotics-oriented evaluation: we isolate a saturation-dominant regime and quantify how standard back-calculation reshapes the transient, including recovery time and overshoot (Sec. 5.4). This provides a grounded baseline for anti-windup-aware gain optimization, where the objective must reflect saturation behavior rather than nominal linear dynamics.

3.3 Data-driven and safe controller tuning

Derivative-free tuning has grown rapidly because it can optimize task-specific objectives even when the plant is hard to model precisely. Bayesian optimization (BO) is attractive for controller tuning because it is sample-efficient and supports noisy, nonconvex objectives via probabilistic surrogate models [10, 11, 20, 30]. Recent control-engineering work demonstrates BO for systematic PID tuning, including multi-loop digital PID design and careful construction of bounded search domains [8, 15, 29].

For robotics, the key challenge is not only efficiency but also *safety*: many candidate gains lead to instability, violent overshoot, or sustained saturation. Safety-aware BO and constrained BO provide mechanisms for restricting evaluations to feasible regions, including probabilistic safety constraints and time-varying formulations [12, 13, 22, 23, 25, 26]. Our hybrid certification (Sec. 4.6) follows this line of work but is intentionally lightweight: it couples analytic PI stability checks with a runtime divergence detector so that unsafe trials are terminated quickly rather than corrupting the BO dataset.

3.4 Simulation benchmarks as hardware surrogates

Because access to physical hardware is often limited, recent robotics research increasingly uses benchmark suites and high-throughput simulation to evaluate robustness under uncertainty and to compare safe tuning methods [16, 17, 21]. Our robustness ensemble and expanded benchmark suite adopt the same philosophy: rather than relying on a single nominal plant, we evaluate gains across uncertainty in dynamics, delays, sensing noise, and actuator limits, and we report both best-case performance and outlier behavior relevant to deployment.

4 Design and methodology

This section specifies the plant and actuator models, discrete-time implementation, saturation handling, and evaluation metrics used throughout the paper. It then derives discrete-time PI stability regions via the Jury criterion under both Euler and exact ZOH discretizations and formalizes the constrained objective used for robust gain selection. These components define the feasibility and scoring framework used in the baseline sweeps, saturation-dominant experiments, Monte Carlo robustness evaluation, and constrained Bayesian optimization results.

4.1 Modeling and discrete-time implementation

4.1.1 Variables and conventions

The input $u(t)$ is the control effort applied to the robotic joint. The output $y(t)$ is the measured joint position. The plant has static gain $K > 0$ and time constant $\tau > 0$. The sampling interval is Δt with sample index k and sample times $t_k = k\Delta t$. The tracking error at sample k is $e_k = r - y_k$. The controller gains are K_p (proportional), K_i (integral), and K_d (derivative).

Unless stated otherwise, constants are $\tau = 1.0$ s, $K = 1.0$, $\Delta t = 0.01$ s, total time $T = 5.0$ s, reference $r = 1$, and clamp $u_k \in [-10, 10]$.

4.1.2 Plant model and continuous-time step response

A first-order LTI model approximates actuator dynamics:

$$\tau \frac{dy(t)}{dt} + y(t) = Ku(t). \quad (1)$$

For a unit-step input $u(t) = 1$ and $y(0) = 0$, the step response is

$$y(t) = K \left(1 - e^{-t/\tau} \right). \quad (2)$$

4.1.3 Forward-Euler discretization

Robotic controllers execute in discrete time. Using a forward-Euler update, the plant becomes:

$$y_{k+1} = y_k + \Delta t \left(-\frac{1}{\tau} y_k + \frac{K}{\tau} u_k \right). \quad (3)$$

The tracking error is $e_k = r - y_k$.

4.1.4 Controller laws

P control:

$$u_k = K_p e_k. \quad (4)$$

PI control:

$$u_k = K_p e_k + K_i I_k, \quad I_{k+1} = I_k + e_k \Delta t. \quad (5)$$

PID control:

$$u_k = K_p e_k + K_i I_k + K_d \frac{e_k - e_{k-1}}{\Delta t}. \quad (6)$$

4.1.5 Actuator saturation, derivative filtering, and discrete anti-windup

In hardware, the actuator saturates:

$$u_k^{\text{sat}} = \text{clip}(u_k, u_{\min}, u_{\max}). \quad (7)$$

The derivative term is well known to amplify measurement noise; practical PID implementations therefore use a filtered derivative (band-limited differentiator) rather than an ideal discrete difference [1, 2]. In our pipeline, the derivative estimate is passed through a first-order low-pass filter; this does not change the conceptual derivations, but it yields behavior closer to embedded practice in the delay/noise experiments.

To explicitly model embedded control under saturation, we include a discrete back-calculation anti-windup augmentation:

$$\begin{aligned} I_{k+1} &= I_k + \Delta t \left(e_k + \frac{u_k^{\text{sat}} - u_k}{K_{aw}} \right), \\ u_k &= K_p e_k + K_i I_k + K_d \frac{e_k - e_{k-1}}{\Delta t}, \end{aligned} \quad (8)$$

where $K_{aw} > 0$ parameterizes an *inverse* correction gain (equivalently, a time constant $T_{aw} = K_{aw}$); larger K_{aw} weakens the correction and $K_{aw} \rightarrow \infty$ recovers the baseline integrator.

4.2 Performance metrics

To compare controllers across gain sweeps and across non-ideal model variants, we report a small set of standard step-response and tracking-fidelity metrics. All metrics are computed from sampled trajectories $\{y_k\}_{k=0}^N$ at times $t_k = k\Delta t$ with reference r .

Percent overshoot (%OS). Overshoot quantifies the maximum peak above the reference during a transient. It is reported as a percentage of r and clipped at zero so monotone responses do not produce negative overshoot:

$$\%OS = \max \left(0, \frac{\max_k(y_k) - r}{r} \right) \cdot 100. \quad (9)$$

For the delay-free first-order plant, overshoot is typically zero in the stable gain range; overshoot becomes meaningful once delay, second-order dynamics, or saturation-driven windup are present.

Rise time (t_r). Rise time measures how quickly the output approaches the target. We use the 90% threshold definition:

$$t_r = \min \{t_k : y_k \geq 0.9r\}. \quad (10)$$

If the trajectory does not reach $0.9r$ within the finite simulation horizon, we report t_r as “–” in tables.

Settling time (t_s). Settling time measures when the trajectory enters and stays within a tight tolerance band around r . We use a strict $\pm 2\%$ band:

$$t_s = \min \{t_k : |y_j - r| \leq 0.02r \ \forall j \geq k\}. \quad (11)$$

If the response never satisfies the band condition over the horizon, we report “–” (and in some plots we annotate as $> T$).

Terminal steady-state error (e_{ss}). Because experiments run for a finite horizon, we estimate terminal tracking error by averaging the absolute error over the last N_{end} samples:

$$e_{ss} \approx \frac{1}{N_{\text{end}}} \sum_{k=N-N_{\text{end}}+1}^N |r - y_k|. \quad (12)$$

Integral of absolute error (IAE). IAE measures cumulative tracking error over the full trajectory and directly penalizes long recovery tails:

$$\text{IAE} \approx \sum_{k=0}^N |e_k| \Delta t. \quad (13)$$

4.3 Discrete-time stability regions for PI control

To connect the PI stability results to the familiar proportional case, consider P control with Euler discretization.

Combining (3) and (4) (with $r = 0$ for stability analysis) yields the scalar closed-loop pole

$$z = 1 - \frac{\Delta t}{\tau} (1 + KK_p), \quad (14)$$

and stability requires $|z| < 1$, which implies $0 < \Delta t < \frac{2\tau}{1+KK_p}$.

The baseline section uses simulations to reveal trends, but safe gain selection for embedded control benefits from *closed-form* stability constraints. For PI control, the closed-loop sampled-data system is second-order, and the Jury criterion provides necessary and sufficient conditions for discrete-time stability [3].

4.3.1 Euler discretization: explicit Jury inequalities

Let $\alpha = \Delta t/\tau$. For stability analysis set $r = 0$ so $e_k = -y_k$. Under Euler discretization, the closed-loop state update for $x_k = [y_k, I_k]^T$ becomes

$$x_{k+1} = \begin{bmatrix} 1 - \alpha(1 + KK_p) & \alpha KK_i \\ -\Delta t & 1 \end{bmatrix} x_k. \quad (15)$$

Let tr and \det be the trace and determinant of the state matrix. The characteristic polynomial is $\lambda^2 - \text{tr} \lambda + \det = 0$. Applying the Jury test for a monic second-order polynomial yields three inequalities:

$$K_i > 0, \quad (16)$$

$$4 - 2\alpha(1 + KK_p) + \alpha KK_i \Delta t > 0, \quad (17)$$

$$\alpha(1 + KK_p) - \alpha KK_i \Delta t > 0. \quad (18)$$

The final inequality can be rearranged into an interpretable guardrail:

$$K_i < \frac{1 + KK_p}{K \Delta t}. \quad (19)$$

Fig. 1 highlights how the integrator-gain guardrail varies with sampling, and why discretization choice changes the admissible K_i at practical Δt .

4.3.2 Exact ZOH discretization

Under a ZOH assumption, the exact discrete plant is $y_{k+1} = ay_k + bu_k$ with $a = e^{-\Delta t/\tau}$ and $b = K(1 - a)$. The closed-loop PI state matrix becomes

$$x_{k+1} = \begin{bmatrix} a - bK_p & bK_i \\ -\Delta t & 1 \end{bmatrix} x_k, \quad (20)$$

and the same Jury logic yields a comparable stability region (Fig. 2).

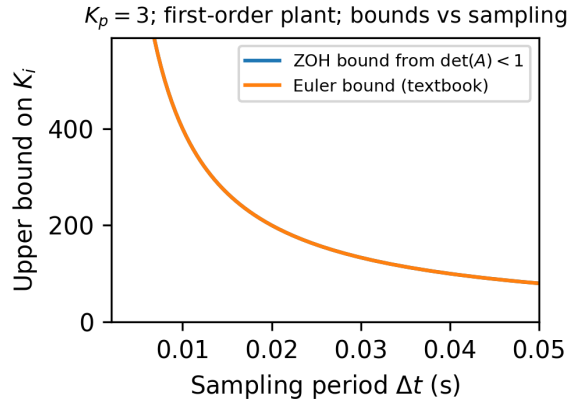


Figure 1: Sampling-period dependence of the integrator gain guardrail for a first-order plant with PI control. The forward-Euler condition in (19) is compared to a ZOH-derived sufficient bound obtained from the discrete-time determinant condition (Sec. III-B).

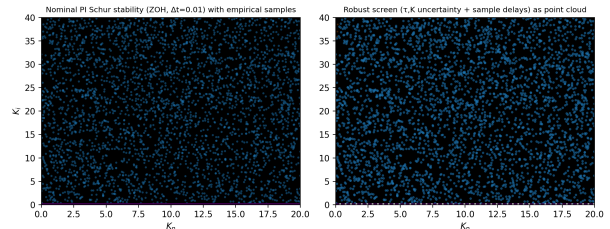


Figure 2: Nominal PI Schur-stable set (ZOH, $\Delta t = 0.01$) and robust point-cloud screen under plant uncertainty and sample delays; sampled gain outcomes are overlaid to validate the analytic boundary.

4.4 Saturation-dominant behavior and anti-windup

To evaluate saturation and windup directly (rather than only in the baseline sweeps), we define a saturation-dominant scenario by (i) tightening the actuator clamp so that early transients saturate, and (ii) adding a small input delay and lightly damped second-order actuator dynamics to emulate realistic servo behavior. In this regime, integral windup is expected to elongate recovery tails unless anti-windup is applied. The experiment reports both the output trajectory and the commanded/saturated effort to directly visualize clamping and recovery.

4.5 Robust constraint-aware gain tuning

To quantify robustness under non-idealities, we evaluate gains across a randomized family of models:

- Uncertain first-order parameters: $\tau \sim \mathcal{U}[0.5, 1.5]$ and

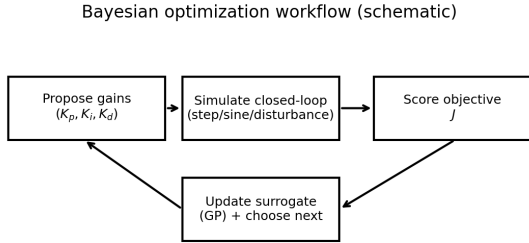


Figure 3: BO workflow: propose gains, evaluate, score J , update surrogate.

$$K \sim \mathcal{U}[0.8, 1.2].$$

- Input delay: $d \in \{0, 1, 2, 3\}$ samples.
- Measurement imperfections: additive noise $\sigma \sim \mathcal{U}[0, 0.01]$ and quantization $\Delta_q \in \{0, 0.001, 0.002\}$.
- Tighter saturation limits: $u_{\max} \in \{2, 3, 5\}$ to trigger clamping in a subset of trials.

Each candidate gain triple is scored by an objective that aggregates both nominal tracking and robustness:

$$J(K_p, K_i, K_d) = \text{median}_{m \in \mathcal{M}} J_m,$$

$$J_m = \text{IAE}_m + \lambda_{os} \max(0, \%OS_m - \%OS_{\max})^2 + \lambda_{sat} \text{sat_duty}_m^2 + \lambda_u u_{\text{rms},m}^2. \quad (21)$$

Parameterization. Unless noted, we set $\%OS_{\max} = 5\%$, $(\lambda_{os}, \lambda_{sat}, \lambda_u) = (1, 5, 0.5)$, and compute all metrics over a 2 s horizon with unit-step reference; IAE is normalized by the horizon length to keep J dimensionless. where \mathcal{M} indexes randomized models and sat_duty_m is the fraction of time the actuator saturates. This objective is compatible with Bayesian optimization (BO) because it is expensive, noisy, and non-convex.

4.6 ML-aided gain tuning via Bayesian optimization

Manual tuning requires iterative trial-and-error. An alternative is to treat the closed-loop evaluation as a black box and optimize gains by minimizing a scalar cost function built from (9)–(13) (or the robust objective in (21)). Bayesian optimization iteratively proposes (K_p, K_i, K_d) , evaluates J , and updates a surrogate model to select the next candidate [10, 11].

4.6.1 Hybrid certification for safe gain exploration

A central risk of black-box gain tuning is evaluating controllers that are numerically stable under saturation yet

Algorithm 1 Hybrid-certified Safe-BO (HC-SBO) for PID gains.

- 1: **Input:** gain bounds \mathcal{B} ; analytic feasible set \mathcal{S} (Jury); behavioral filter \mathcal{F} (short-horizon check); robust objective $J(\cdot)$; initial budget n_0 ; total budget N .
- 2: Sample n_0 points from \mathcal{B} until each satisfies $x \in (\mathcal{S} \cap \mathcal{F})$; evaluate $J(x)$.
- 3: **for** $n = n_0$ to $N - 1$ **do**
- 4: Fit GP surrogate \hat{J} .
- 5: Draw candidate pool $\mathcal{C} \subset \mathcal{B}$ and keep only feasible candidates $\mathcal{C} \leftarrow \{x \in \mathcal{C} : x \in \mathcal{S} \cap \mathcal{F}\}$.
- 6: Choose $x_{n+1} = \arg \max_{x \in \mathcal{C}} \text{EI}(x; \hat{J})$.
- 7: Evaluate $J(x_{n+1})$ and update dataset.
- 8: **end for**
- 9: **Output:** best gains observed.

dynamically unacceptable (e.g., extreme overshoot, sustained saturation, or long windup recovery). We introduce a hybrid certification filter that prevents such evaluations while retaining sample efficiency:

- **Analytic feasibility (stability):** we restrict candidates to the ZOH Jury-feasible PI region \mathcal{S} derived in Sec. 4.3. This provides a conservative, interpretable guardrail for sampled-data stability of the nominal first-order joint model.
- **Behavioral certification (constraints):** we additionally require that a short-horizon nominal check on a second-order actuator model satisfies bounded overshoot and does not remain saturated for the entire transient. This rejects aggressively destabilizing gains before expensive robust evaluation.

This filter is lightweight and evaluation-driven: it enforces robotics-relevant behavior constraints rather than merely preventing divergence.

PI guard vs. PID tuning. The analytic Jury guard applies to the PI pair (K_p, K_i) and is used as a conservative pre-filter; the derivative term is safeguarded by the behavioral screen and the robust evaluation stage.

4.6.2 Actuator-realistic second-order joint model

The first-order plant in (1) captures a velocity-limited actuator, but many robotic joints exhibit second-order behavior dominated by inertia and damping. To emulate this, we evaluate gains on the normalized second-order actuator model

$$\ddot{\theta}(t) + 2\zeta\omega_n\dot{\theta}(t) + \omega_n^2\theta(t) = K_u u(t) + d(t), \quad (22)$$

where θ is joint position, (ω_n, ζ) set natural frequency and damping, K_u maps input to torque/acceleration, and $d(t)$ is a disturbance torque. We augment (22) with practical

non-idealities: (i) input delay of 1–2 samples, (ii) Coulomb and viscous friction, (iii) a small deadzone, (iv) encoder quantization and additive noise, and (v) tight saturation that makes anti-windup essential. This model bridges a single-pole surrogate and actuator behavior commonly observed in robotics.

4.6.3 Expanded robust benchmark suite

We define a robust benchmark that combines (A) the ZOH-discretized first-order joint and (B) the second-order actuator model (22). For each family, parameters are sampled from bounded uncertainty sets and evaluated under three tasks: step tracking, sinusoidal tracking, and disturbance rejection. The reported objective is the median score over draws and tasks; it aggregates tracking error (IAE/RMSE), overshoot penalties, and control-effort penalties.

5 Experiments and results

This section reports baseline gain sweeps and then progressively more realistic evaluation results (saturation-dominant tests, Monte Carlo robustness, and expanded benchmark BO results).

5.1 Evaluation validity and scope

The results are reported as comparative outcomes under a consistent evaluation protocol. All controllers are executed in discrete time with ZOH actuation and explicit effort clamping, and all candidate gains are tested against non-idealities that commonly dominate PID performance: sample delay, measurement noise, encoder quantization, and tighter saturation limits (Sec. 4.5). In addition to a first-order surrogate, gains are evaluated on a lightly damped second-order actuator family with friction and deadzone (Sec. 4.6.2). These evaluations quantify typical behavior and violation rates under uncertainty rather than relying on a single nominal trajectory.

5.2 Experimental design (baseline)

We perform three sweeps:

- P only: $K_p \in \{0.5, 1.0, 1.5, 2.0, 3.0\}$ with $K_i = 0$, $K_d = 0$.
- PI: fix $K_p = 3.0$ and vary $K_i \in \{0.00, 0.25, 0.50, 1.00\}$ with $K_d = 0$.
- PID: fix $K_p = 3.0$, $K_i = 1.0$ and vary $K_d \in \{0.00, 0.05, 0.10\}$.

For each run we log t_k , y_k , u_k , and e_k , compute the metrics in (9)–(13), and produce plots and tables.

Table 2: Modeled non-idealities used to emulate embedded joint control.

Non-ideality	Why it matters	How modeled (this paper)	
Effort saturation	current/voltage limits cause nonlinear recovery and windup	hard saturation	clamp $u \in [u_{\min}, u_{\max}]$; saturation-dominant setting tightens bounds (Sec. 4.4)
Sample delay	compute/communication delay reduces phase margin	$\mathfrak{h} \in \{0, 1, 2, 3\}$ samples	in robustness ensemble
Noise & quantization	sensors/encoders inject jitter; K_d can amplify it	additive noise $\sigma \sim \mathcal{U}[0, 0.01]$ and quantization $\Delta_q \in \{0, 0.001, 0.002\}$	(Sec. 4.5)
Second-order dynamics	motors/links add lightly damped modes	actuator family in (22) with (ω_n, ζ) and input gain K_u (Sec. 4.6.2)	
Friction & deadzone	stiction and Coulomb friction distort small motions	viscous $b = 0.05$ – 0.06 , Coulomb $f_c = 0.02$ – 0.03 , small deadzone	(Table 7)

Table 3: P-only step-response metrics ($K_i = 0$, $K_d = 0$).

K_p	%OS	t_r (s)	t_s (s)	e_{ss}	IAE
0.5	0.0000	–	–	0.6669	3.5495
1.0	0.0000	–	–	0.5000	2.7419
1.5	0.0000	–	–	0.4000	2.2306
2.0	0.0000	–	–	0.3333	1.8787
3.0	0.0000	–	–	0.2500	1.4263

5.3 Results (baseline characterization)

5.3.1 Proportional-only control

Figs. 4 and 5 illustrate monotone convergence and the expected reduction of the steady-state tail as K_p increases. Overshoot is identically zero across this sweep for the delay-free single-pole plant.

For a stable first-order plant without delay, P control produces a monotone, non-oscillatory transient because the closed-loop dynamics remain first-order. The key limitation is the nonzero steady-state error: with $u = K_p(r - y)$ and plant DC gain K , the closed-loop DC gain is $\frac{KK_p}{1+KK_p}$, so for a unit step $r = 1$ the asymptotic output is $y_\infty = \frac{KK_p}{1+KK_p}$ and the steady-state error is $e_\infty = \frac{1}{1+KK_p}$. This

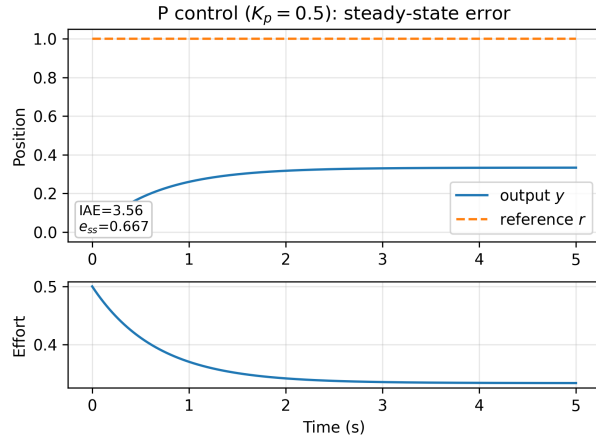


Figure 4: P-only step response at $K_p = 0.5$.

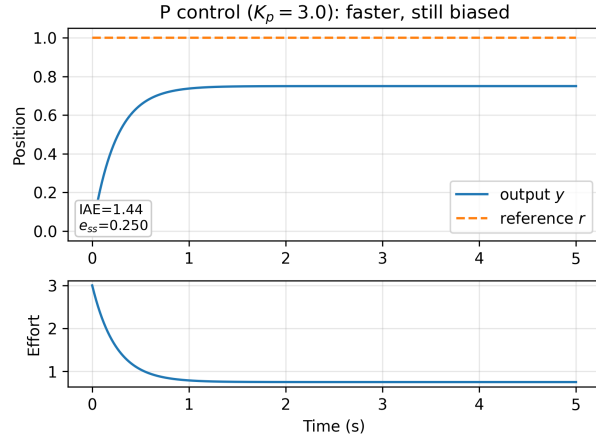


Figure 5: P-only step response at $K_p = 3.0$.

Table 4: PI step-response metrics at $K_p = 3.0$ ($K_d = 0$).

K_i	%OS	t_r (s)	t_s (s)	e_{ss}	IAE
0.00	0.0000	—	—	0.2500	1.4263
0.25	0.0000	—	—	0.1786	1.2159
0.50	0.0000	—	—	0.1257	1.0419
1.00	0.0000	2.7800	—	0.0590	0.7789

directly explains the trend in Table 3: as K_p increases, e_{ss} decreases approximately like $\frac{1}{1+K_p}$ for $K = 1$, and IAE decreases because the tail area shrinks.

5.3.2 Proportional-integral control

Fig. 6–Fig. 8 visualize the effect of increasing K_i at fixed $K_p = 3.0$.

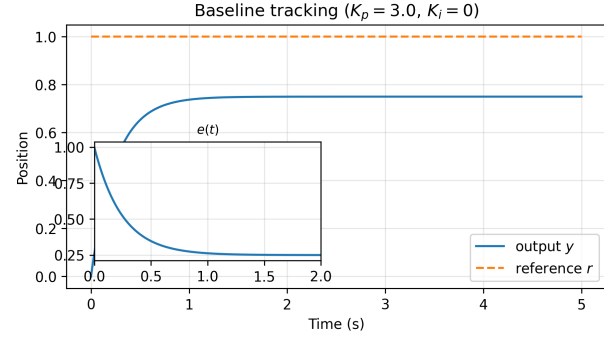


Figure 6: Baseline ($K_p = 3.0, K_i = 0$).

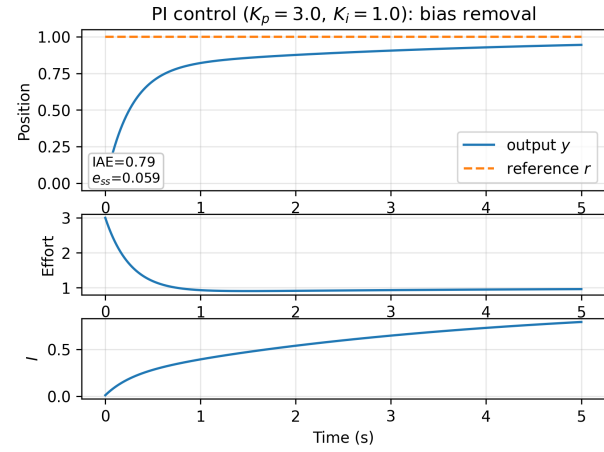


Figure 7: PI at $K_p = 3.0, K_i = 1.0$.

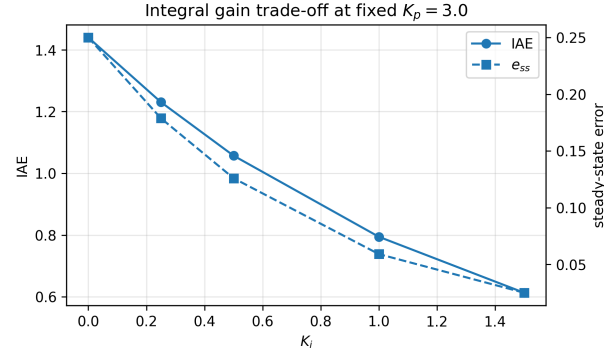


Figure 8: IAE vs. K_i at $K_p = 3.0$.

5.3.3 Full PID control

Figs. 9–10 separate two regimes. On a delay-free single-pole plant, changing K_d has only a second-order influence relative to K_p and K_i (Fig. 9). Once higher-order actuator dynamics and a few samples of delay are introduced, derivative action becomes measurably useful for damping and transient shaping (Fig. 10). For readability, the three step-response traces are merged into a single figure.

Table 5: PID step-response metrics at $K_p = 3.0$, $K_i = 1.0$.

K_d	%OS	t_r (s)	t_s (s)	e_{ss}	IAE
0.00	0.0000	2.7800	—	0.0590	0.7789
0.05	0.0000	2.7300	—	0.0580	0.7831
0.10	0.0000	2.6800	—	0.0570	0.7873

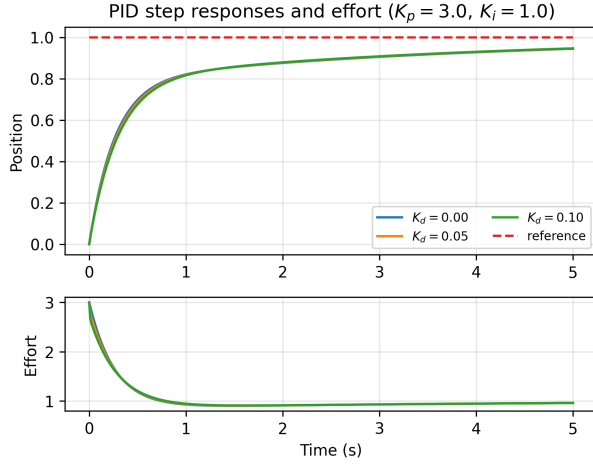


Figure 9: PID step responses at $K_p = 3.0$, $K_i = 1.0$, varying K_d (merged).

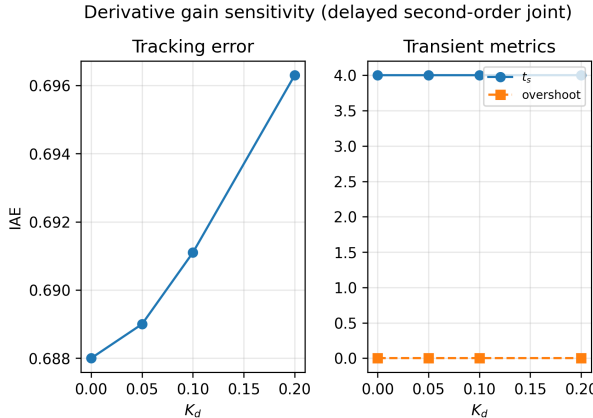


Figure 10: Derivative gain sensitivity under a delayed second-order joint model: IAE (left) and transient metrics (right) vs. K_d .

5.4 Saturation-dominant results and anti-windup

Figs. 11–12 report the saturation-dominant scenario described in Sec. 4.4. This test forces the actuator to clamp during the early transient so that, without compensation, the integrator would otherwise accumulate error while the input is pinned at its limit.

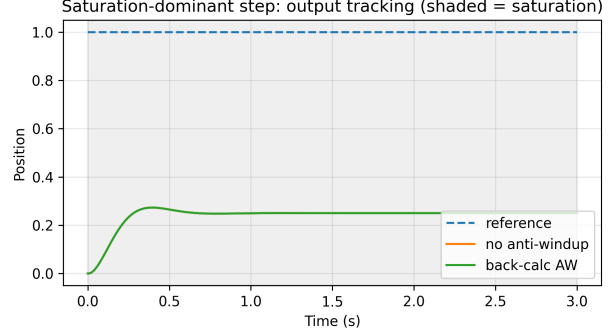


Figure 11: Saturation-dominant (output).

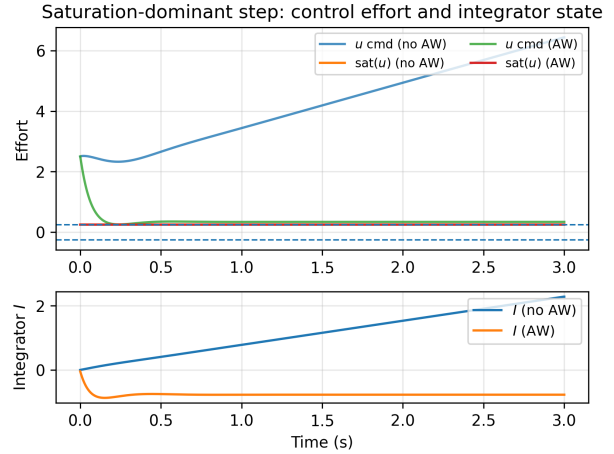


Figure 12: Saturation-dominant (effort).

Table 6: Monte Carlo robustness summary over a family of joint models (ZOH discretization, randomized τ , K , delay, noise, quantization, and saturation limits).

Controller	K_p	K_i	K_d	Median IAE	Median OS (%)	Median sat duty
Manual	3.000	1.000	0.050	0.687	0.000	0.000
Robust-tuned	10.000	25.000	0.800	0.470	1.000	0.000

5.5 Monte Carlo robustness results

We next evaluate the same controller family under the randomized model distribution described in Sec. 4.5. This test probes whether a gain choice that performs well on the nominal model continues to behave acceptably under uncertainty in (τ, K) , sample delay, measurement noise/quantization, and tighter saturation limits.

Table 6 summarizes the median performance across the model family for a manual baseline and a robustness-oriented tuned controller.

5.6 Expanded-benchmark Safe-BO results

We now report results for the hybrid-certified Safe-BO workflow described in Sec. 4.6 when evaluated on the ex-

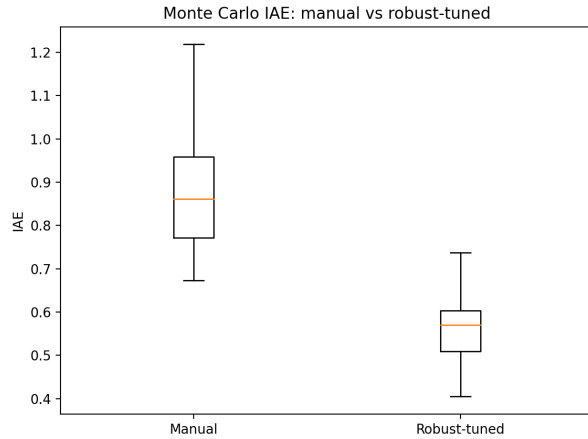


Figure 13: Monte Carlo IAE: manual vs robust-tuned.

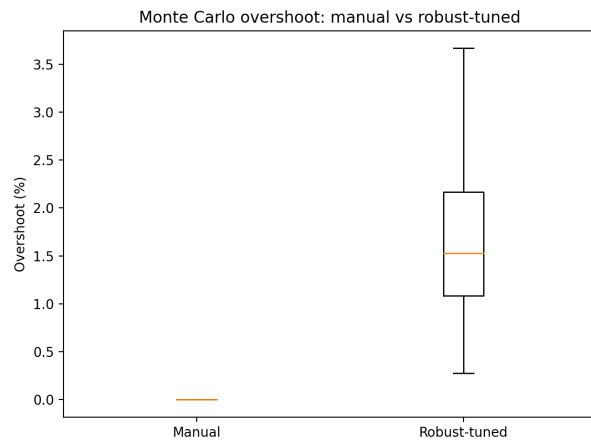


Figure 14: Monte Carlo overshoot: manual vs robust-tuned.

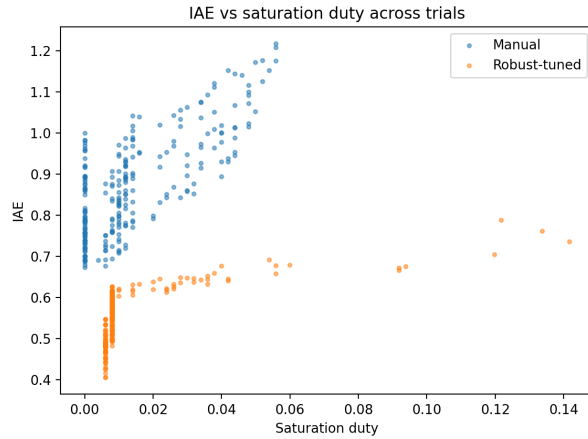


Figure 15: IAE vs saturation duty across trials.

expanded benchmark suite (first-order ZOH family + second-

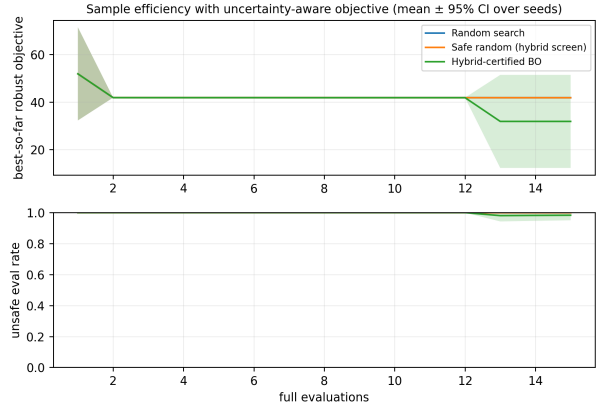


Figure 16: Expanded benchmark: best-so-far robust objective vs. evaluations (mean \pm 95% CI over seeds, top) and unsafe evaluation rate (bottom).

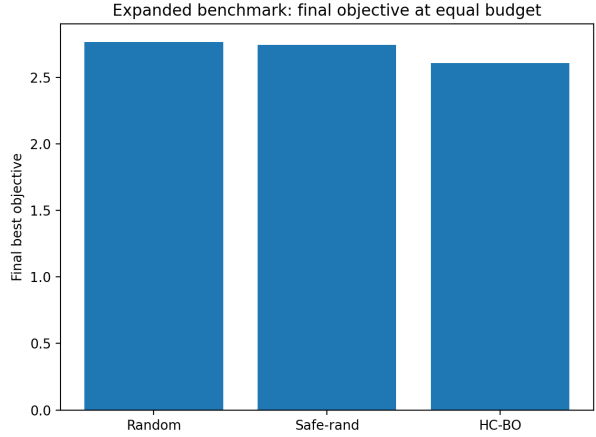


Figure 17: Expanded benchmark: final objective at equal budget.

order actuator family). This experiment addresses two practical questions: (i) does the certification filter prevent clearly unacceptable evaluations while still allowing progress, and (ii) does the constrained workflow remain sample-efficient compared to unconstrained search?

6 Discussion

Baseline sweeps confirm that for a delay-free first-order plant, K_p primarily sets the steady-state tail (but cannot remove steady-state error), and K_i dominates tail removal and IAE reduction. On this nominal single-pole system, derivative action yields only modest shaping; however, once delay and higher-order actuator dynamics are introduced, K_d becomes materially beneficial for damping and transient control. The stability-region derivations provide a fast guardrail for PI gains before evaluation, and the

Table 7: Representative second-order actuator family used for the benchmark plots (Figs. 18–21).

Parameter	Value (nominal)
Natural frequency ω_n	8–10 rad/s
Damping ratio ζ	0.6–0.8
Input gain K_u	1.0
Sample period Δt	2 ms
Input saturation u_{\max}	1.0 (step/sine), 0.25 (AW ablation)
Sample delay	1 sample
Friction	viscous $b = 0.05–0.06$, Coulomb f_i
Reference	unit step or $0.5 \sin(2\pi \cdot 0.8t)$

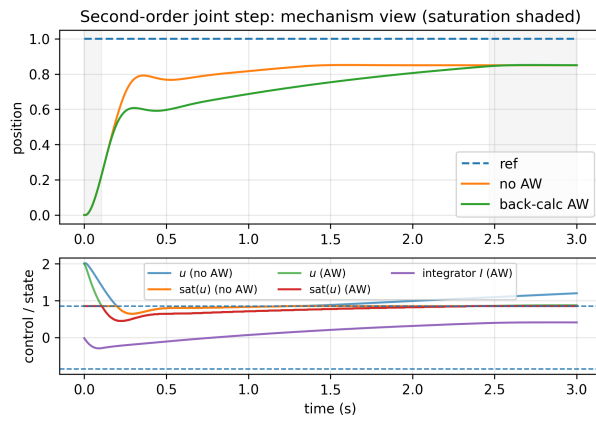


Figure 18: Second-order actuator benchmark (step): output tracking with saturation intervals shaded (top) and corresponding commanded/saturated control plus integrator state (bottom), comparing no anti-windup vs. back-calculation.

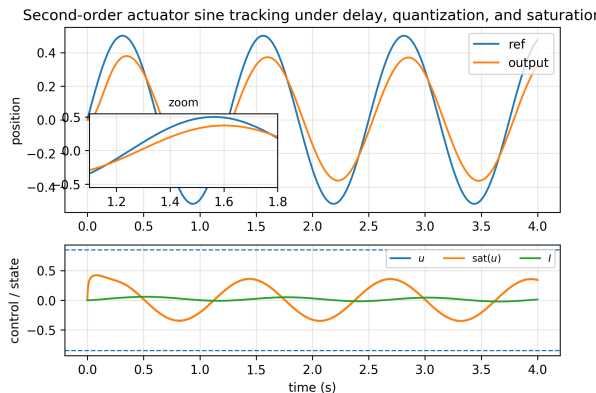


Figure 19: Second-order actuator benchmark (sine): tracking under delay, quantization, and saturation (top, with inset zoom) and corresponding commanded/saturated control plus integrator state (bottom).

saturation-dominant tests demonstrate why anti-windup is essential once the clamp is active. Robustness-oriented

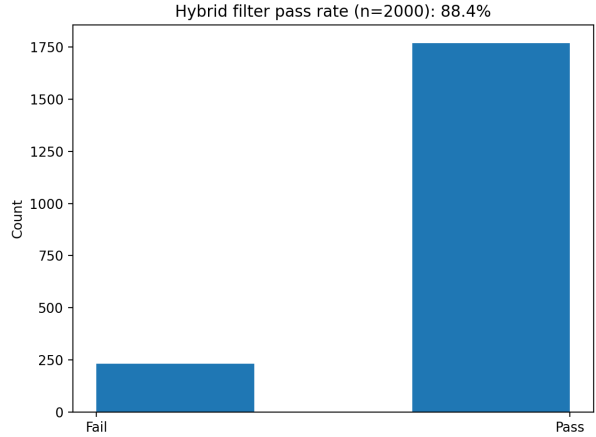


Figure 20: Feasible fraction passing hybrid filter.

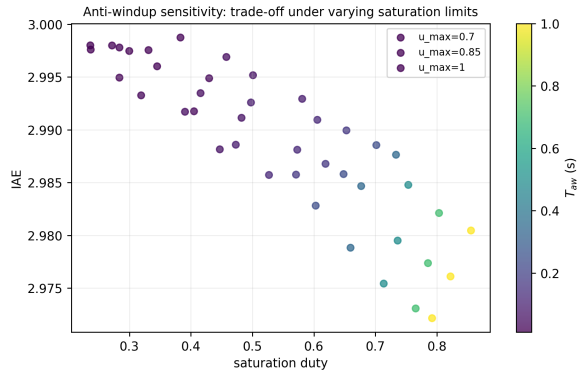


Figure 21: Anti-windup sensitivity as a trade-off between IAE and saturation duty across back-calculation time constants T_{aw} (color) and multiple saturation limits u_{\max} .

tuning and Safe-BO results illustrate a practical workflow for constrained tuning: optimizing gains against randomized model families improves typical-case tracking while keeping overshoot bounded and rejecting a large fraction of unsafe candidate gains.

6.1 Limitations and threats to validity

The results emphasize that sampling, saturation, and small delays change both the safe gain set and the qualitative closed-loop behavior, even for simple plants. The ZOH and Euler PI regions provide an interpretable first-line guardrail for the integral action that most strongly governs steady-state and tail behavior.

Scope. The analytic guard is nominal and PI-specific; for full PID tuning we therefore rely on the behavioral screen and robust evaluation, and we report evaluation-based evidence rather than hardware guarantees. We explicitly model uncertainty, delay, noise, and quantization to approximate common embedded joint loops, but the

benchmark models remain simplified abstractions.

7 Conclusion

This paper reformulates a classic PID tuning problem in the practical setting of discrete-time embedded control with actuator limits. In addition to baseline P/PI/PID characterization, we derive PI stability regions using the Jury criterion, demonstrate saturation-dominant anti-windup behavior, and propose a robustness-oriented tuning workflow that emulates key non-idealities through a randomized model family. We further introduce a hybrid-certified Safe-BO workflow to prevent unsafe gain exploration and demonstrate its behavior on a second-order actuator benchmark suite.

A Exact zero-order-hold discretization

Forward Euler is simple and matches many educational implementations, but a first-order LTI plant also admits an exact discrete-time update under a ZOH assumption:

$$y_{k+1} = a y_k + b u_k, \quad a = e^{-\Delta t/\tau}, \quad b = K \left(1 - e^{-\Delta t/\tau}\right). \quad (23)$$

B Implementation notes for embedded robotic joints

This section summarizes practical details that materially affect digital PID behavior but are often omitted in simplified analyses.

B.1 Derivative filtering and noise

The derivative term amplifies measurement noise. In embedded implementations, a first-order low-pass filter (“dirty derivative”) is commonly used:

$$D(s) = \frac{K_d s}{1 + \frac{s}{\omega_f}}, \quad (24)$$

implemented in discrete time using a stable recursion. In our evaluation studies, adding measurement noise shifts the trade-off between overshoot and IAE, and derivative action becomes beneficial only when the effective bandwidth is chosen relative to the sampling period and noise level. As a practical guideline, we recommend selecting ω_f such that $\omega_f T_s \in [0.1, 0.3]$ and evaluating robustness under noise/quantization before increasing K_d .

B.2 Anti-windup tuning and saturation duty

Back-calculation anti-windup introduces an additional time constant T_{aw} (or gain K_{aw}). Setting T_{aw} too small can reintroduce aggressive behavior near saturation; setting it too large yields slow recovery tails. We therefore report a saturation-duty metric (fraction of time in saturation) alongside IAE and overshoot, and we treat “low duty + low IAE” as a robustness indicator under tighter effort limits.

B.3 Delay, quantization, and discrete-time guards

Computational delay and quantization act like additional dynamics that reduce phase margin. We therefore propose using analytic discrete-time stability guards (Jury conditions) as a prefilter for any automated tuning loop, and then validating candidates under randomized uncertainty (delay, quantization, noise) before declaring a gain set robust.

B.4 Reproducibility checklist

- Plant model family and uncertainty bounds: (K, τ) ranges; delay/jitter distribution; noise and quantization levels.
- Digital implementation: sampling period T_s ; discretization method (Euler/ZOH); derivative filter (ω_f); anti-windup form and parameter (T_{aw} or K_{aw}).
- Actuator constraints: saturation bounds u_{\max} (and any rate limits if used); definition of saturation duty.
- Task definition: reference trajectory, horizon length, and any disturbances/payload changes.
- Metrics: IAE definition and normalization; overshoot threshold; penalties/weights; early-termination rules for unsafe trials.
- Optimization protocol: candidate bounds, initial design size, BO kernel/acquisition, and random seeds.

B.5 Objective design for tuning

Robotics PID tuning is frequently framed as “make tracking good,” but the objective choice strongly influences the resulting gains. A pure tracking-error objective tends to push gains toward aggressive behavior that exploits saturation, whereas adding explicit penalties on effort and effort rate discourages chattering and reduces thermal stress. In this work, we evaluate candidates under a composite objective that includes IAE, overshoot, and a saturation-duty term; this combination yields a predictable trade-off between tracking performance and saturation exposure.

B.6 Reporting standards for reproducible tuning

For papers that propose tuning procedures (manual or automated), we recommend reporting: the target trajectory, the error metric (and whether it is absolute/squared), the evaluation horizon, saturation bounds, sampling period, delay model, and sensor quantization/noise assumptions. Without these details, it is difficult to interpret whether a reported “better” controller is due to a tuning method or due to a different experimental setup.

C Jury-test coefficients for PI with ZOH

For completeness, we outline the coefficient mapping used for the ZOH-discretized first-order plant. Let $G(s) = \frac{K}{\tau s + 1}$ and let the ZOH equivalent at sampling period T_s be

$$G(z) = \frac{K(1 - e^{-T_s/\tau})}{z - e^{-T_s/\tau}}. \quad (25)$$

With the discrete PI controller $C(z) = K_p + K_i \frac{T_s z}{z - 1}$, the closed-loop characteristic polynomial can be written in the monic form

$$p(z) = z^2 + a_1 z + a_0, \quad (26)$$

where a_1 and a_0 are affine functions of (K_p, K_i) for fixed (τ, T_s) . The Jury stability test for a second-order polynomial reduces to three inequalities:

$$1 + a_1 + a_0 > 0, \quad 1 - a_1 + a_0 > 0, \quad 1 - a_0 > 0. \quad (27)$$

These constraints define a convex polygon in the (K_p, K_i) plane and serve as an analytic prefilter in our hybrid-certified search.

D Hybrid-certified Bayesian optimization procedure

We summarize the hybrid-certified tuning workflow used in our experiments.

1. **Define** a feasible gain box for (K_p, K_i, K_d) and implementation parameters (sampling period T_s , derivative filter bandwidth ω_f , and anti-windup time constant T_{aw}).
2. **Analytic prefilter:** reject any candidate that violates the discrete-time stability guards derived for the nominal model (Jury conditions for PI, and corresponding linearized constraints for PID).

3. **Behavioral check:** run a short-horizon evaluation on a small subset of uncertain models. Reject candidates that produce divergence, excessive overshoot, or persistent saturation.
4. **Robust scoring:** evaluate remaining candidates on a larger uncertainty set and compute a robust objective (median IAE plus penalties in this paper; a risk-averse CVaR variant can be substituted when tail performance dominates).
5. **BO update:** update the Gaussian-process surrogate and propose the next candidate, repeating until the evaluation budget is exhausted.

This structure preserves BO’s data efficiency while enforcing stability and practicality constraints that are critical for robotic joints.

References

- [1] R. P. Borase, D. K. Maghade, S. Y. Sondkar, and S. N. Pawar, “A review of PID control, tuning methods and applications,” *ISA Transactions*, vol. 120, pp. 68–97, 2021.
- [2] Z. Zhang, K. H. Ang, S. Y. Li, and Y. C. Chong, “PID control system analysis and design for sampled-data systems,” *Annual Reviews in Control*, vol. 55, pp. 196–214, 2023.
- [3] M. S. Fadali and A. Vissioli, *Digital Control Engineering: Analysis and Design*, 3rd ed. London, U.K.: Academic Press, 2020.
- [4] M. C. Turner and D. J. Richards, “Two-stage anti-windup compensation for linear systems with actuator saturation,” *International Journal of Control*, vol. 97, no. 4, pp. 751–766, 2024.
- [5] L. L. Leal, V. S. da Silva, and E. A. B. da Silva, “Analytical tuning for double back-calculation anti-windup compensation,” *European Journal of Control*, vol. 55, pp. 89–101, 2020.
- [6] P. Borja, J. van der Veen, and J. M. A. Scherpen, “Trajectory tracking for robotic arms with input saturation and only position measurements,” in *Proc. IEEE Conf. Decision and Control (CDC)*, 2021.
- [7] L. Roveda, N. P. Fantuzzi, and D. Piga, “Bayesian optimization for robot trajectory tracking control,” *Journal of Intelligent Manufacturing*, vol. 31, pp. 503–516, 2020.

[8] S. Coutinho, G. A. de Oliveira, and R. M. Palhares, “Automatic tuning of digital multi-loop PID controllers using Bayesian optimization,” *Control Engineering Practice*, vol. 132, p. 105430, 2023.

[9] Z. Wang, “Gaussian processes for machine learning: A tutorial,” *arXiv:2009.10862*, 2021.

[10] R. Garnett, *Bayesian Optimization*. Cambridge, U.K.: Cambridge University Press, 2023.

[11] Z. Wang and S. Jegelka, “A survey of Bayesian optimization,” *ACM Computing Surveys*, vol. 55, no. 13s, pp. 1–36, 2023.

[12] D. Eriksson and M. Poloczek, “Scalable constrained Bayesian optimization,” in *Proc. Int. Conf. Artificial Intelligence and Statistics (AISTATS)*, 2021.

[13] F. Berkenkamp, R. Moriconi, A. P. Schoellig, and A. Krause, “Safe and automatic parameter tuning in robotics,” *Machine Learning*, vol. 110, pp. 2673–2702, 2021.

[14] H. Cho and E. Frazier, “Time-varying Bayesian optimization,” in *Proc. Int. Conf. Artificial Intelligence and Statistics (AISTATS)*, 2022.

[15] M. Zagorowska, “Automatic tuning of control engineering algorithms with Bayesian optimization,” Ph.D. dissertation, RWTH Aachen University, 2025.

[16] H. Yuan, J. H. Nguyen, and S. S. Sastry, “Safe-Control-Gym: A unified benchmark suite for safe learning-based control and reinforcement learning in robotics,” *IEEE Robotics and Automation Letters*, vol. 7, no. 2, pp. 1114–1121, 2022.

[17] J. A. Mower, E. Lavigne, and P. Long, “ROS-PyBullet interface (RoPI): A framework for benchmarking robotics simulators,” *arXiv:2208.07387*, 2022.

[18] E. Coumans, “Bullet physics simulation,” in *ACM SIGGRAPH 2015 Courses*, 2015.

[19] E. Coumans and Y. Bai, “PyBullet, a Python module for physics simulation for games, robotics and machine learning,” 2016. [Online]. Available: <https://pybullet.org>

[20] M. Balandat *et al.*, “BoTorch: A framework for efficient Monte-Carlo Bayesian optimization,” in *Advances in Neural Information Processing Systems (NeurIPS)*, 2020.

[21] V. Makoviychuk *et al.*, “Isaac Gym: High performance GPU-based physics simulation for robot learning,” *arXiv:2108.10470*, 2021.

[22] L. Widmer, Y. Kang, S. Sukhija, J. Hübotter, A. Krause, and M. Hutter, “Tuning legged locomotion controllers with Bayesian optimization,” in *Proc. Conf. on Robot Learning (CoRL)*, 2023.

[23] R. von Rohr, N. Solowjow, A. Krause, and A. Hutter, “Local Bayesian optimization for controller tuning with crash constraints,” *Automatisierungstechnik*, vol. 72, no. 1, pp. 12–22, 2024.

[24] H. Cho and E. Frazier, “A run-indexed Gaussian process bandit for time-varying Bayesian optimization,” in *Proc. Int. Conf. Machine Learning (ICML)*, 2024.

[25] D. Brunzema, J. Huang, and N. Dall’Anese, “Time-varying Bayesian optimization for non-stationary systems,” in *Proc. IEEE Conf. Decision and Control (CDC)*, 2022.

[26] M. König, A. Vogler, A. Peters, and M. A. Müller, “Risk-averse Gaussian process optimization for safe controller tuning,” *IEEE Robotics and Automation Letters*, vol. 8, no. 7, pp. 4141–4148, 2023.

[27] L. Brunke, M. Greeff, A. Hall, Z. Yuan, S. Zhao, and A. W. Edwards, “Safe learning in robotics: From learning-based control to safe reinforcement learning,” *Annual Review of Control, Robotics, and Autonomous Systems*, vol. 5, pp. 411–444, 2022.

[28] K. P. Wabersich and M. N. Zeilinger, “A predictive safety filter for learning-based control of constrained nonlinear dynamical systems,” *Automatica*, vol. 129, p. 109597, 2021.

[29] E. Khosravi, A. K. Paul, and M. M. Seron, “Performance-driven cascade controller tuning using Bayesian optimization,” in *Proc. IFAC World Congress*, 2020.

[30] S. Fujimoto, A. Konno, and R. Mizuno, “A review of Bayesian optimization in control engineering: A reference and a tutorial,” *Asian Journal of Control*, vol. 25, no. 6, pp. 2265–2291, 2023.

[31] D. Catenaro, L. Rossi, and P. Falconi, “Efficient Bayesian optimization for controller tuning with application to motion control,” *IFAC-PapersOnLine*, vol. 58, no. 6, pp. 508–513, 2024.

[32] H. Wang, Y. Zhang, and L. Xie, “Adaptive event-triggered anti-windup control for saturated switched systems with time delay,” *Automatica*, 2025.

[33] I. Tejado, L. Martínez, and B. M. Vinagre, “Neuron-based back-calculation anti-windup strategy for PID controllers: Improving control performance under actuator saturation,” in *Proc. European Control Conference (ECC)*, 2024.

- [34] E. Çelik, B. K. Taşpınar, and M. S. Erol, “A PID auto-tuning framework applied on mobile robots,” arXiv:2505.03159, 2025.
- [35] A. Çelik, B. K. Taşpınar, and M. S. Erol, “Heteroscedastic Bayesian optimization-based dynamic PID tuning for accurate and robust UAV trajectory tracking,” in *Proc. IEEE/RSJ Int. Conf. on Intelligent Robots and Systems (IROS)*, 2025.
- [36] H. Krasowski, J. Klink, and M. P. Deisenroth, “Provably safe reinforcement learning: Conceptual analysis, survey, and benchmarking,” *Transactions on Machine Learning Research*, 2023.
- [37] W. Xiao, C. G. Cassandras, and D. V. Dimarogonas, “Control barrier functions: System-theoretic foundations and numerical methods,” *Annual Reviews in Control*, vol. 54, pp. 405–423, 2022.
- [38] B. Tearle, K. P. Wabersich, and M. N. Zeilinger, “A predictive safety filter for learning-based racing control,” in *Proc. IEEE Int. Conf. on Robotics and Automation (ICRA)*, 2021.
- [39] G. Costa, J. Pinho, L. Hewing, A. Liniger, and M. N. Zeilinger, “Online learning of MPC for autonomous racing,” *Robotics and Autonomous Systems*, vol. 167, p. 104469, 2023.